Journal of Organometallic Chemistry 694 (2009) 103–112

Contents lists available at ScienceDirect

Journal of Organometallic Chemistry

journal homepage: www.elsevier.com/locate/jorganchem

Synthesis, characterization and electrochemical behavior of some *N*-heterocyclic carbene-containing active site models of [FeFe]-hydrogenases

Li-Cheng Song *, Xiang Luo, Yong-Zhen Wang, Bin Gai, Qing-Mei Hu

Department of Chemistry, State Key Laboratory of Elemento-Organic Chemistry, Nankai University, Tianjin 300071, China

ARTICLE INFO

Article history:
Received 6 August 2008
Received in revised form 7 October 2008
Accepted 9 October 2008
Available online 17 October 2008

Keywords:
[FeFe]-Hydrogenases
N-Heterocyclic carbene
Crystal structure
Biomimetic chemistry
Hydrogen evolution

ABSTRACT

Treatment of parent compounds $[(\mu\text{-}SCH_2)_2X]Fe_2(CO)_6$ (**A**, X = O; **B**, X = NBu-*t*; **C**, X = NC_6H_4OMe-*p*) with *N*-heterocyclic carbene I_{Mes} (I_{Mes} = 1,3-bis(mesityl)imidazol-2-ylidene) generated in situ through reaction of imidazolium salt I_{Mes} ·HCl with *n*-BuLi or *t*-BuOK afforded the monocarbene-substituted complexes $[(\mu\text{-}SCH_2)_2X]Fe_2(CO)_5(I_{Mes})$ (**1**, X = O; **2**, X = NBu-*t*; **3**, X = NC_6H_4OMe-*p*). Similarly, the monocarbene and dicarbene-substituted complexes $[(\mu\text{-}SCH_2)_2NBu\text{-}t]Fe_2(CO)_5[I^*_{Mes}(CH_2)_3I^*_{Mes}]\cdot HBr$ (**4**) and $[(\mu\text{-}SCH_2)_2\text{-}CH_2Fe_2(CO)_5]_2[\mu\text{-}I^*_{Mes}(CH_2)_3I^*_{Mes}]$ (**5**, I^*_{Mes} = 1-(mesityl)imidazol-2-ylidene) could be prepared by reactions of parent compound **B** with the mono-NHC ligand-containing imidazolium salt $[I^*_{Mes}(CH_2)_3I^*_{Mes}]\cdot HBr$ and parent compound $[(\mu\text{-}SCH_2)_2CH_2]Fe_2(CO)_6$ (**D**) with di-NHC ligand $I^*_{Mes}(CH_2)_3I^*_{Mes}$ (both NHC ligands were generated in situ from reaction of *n*-BuLi with imidazolium salt $[I^*_{Mes}I^*_{Mes}(CH_2)_3I^*_{Mes}]\cdot 2HBr$), respectively. The imidazolium salt $[I^*_{Mes}(CH_2)_3I^*_{Mes}]\cdot 2HBr$ was prepared by reaction of 1-(mesityl)imidazole with $Br(CH_2)_3Br$. All the new model compounds **1**–**5** and imidazolium salt $[I^*_{Mes}(CH_2)_3I^*_{Mes}]\cdot 2HBr$ were fully characterized by elemental analysis, spectroscopy, and X-ray crystallography. On the basis of electrochemical studies of **1** and **2**, compound **2** was found to be a catalyst for proton reduction to hydrogen. In addition, an EECC mechanism for this electrocatalytic reaction is preliminarily suggested.

1. Introduction

Hydrogenases are natural enzymes found in several microorganisms that catalyze the production and consumption of hydrogen via the reversible reaction: $H_2 \rightleftharpoons 2H^+ + 2e$ [1–4]. Among the three types of hydrogenases known to date [5,6], [FeFe]-hydrogenases have attracted special attention because of their unusual structures and particularly their extremely high catalytic capability for production of the "clean" and efficient hydrogen fuel [7–9]. X-ray crystallographic [10–13] and FTIR spectroscopic [14–16] studies revealed that the active site of [FeFe]-hydrogenases (so-called H-cluster) consists of a butterfly $[Fe_2S_2]$ subcluster linked to a cubane-like $[Fe_4S_4]$ subcluster via the sulfur atom of a cysteinyl group (Chart 1).

The well-elucidated structure regarding the active site of [FeFe]-hydrogenases has greatly accelerated the designed synthesis of the H-cluster models. It is known that most of the models prepared so far are diiron propanedithiolate (PDT) and azadithiolate (ADT) all-carbonyl complexes, as well as their phosphine-substituted derivatives [17–31]. Recently, the application of *N*-heterocyclic carbenes (NHCs) as surrogates for phosphines to make the NHC ligand-containing model complexes has received considerable attention [32–36]. This is largely because NHC ligands have stronger σ-donation with negligible π-accepting ability and greater electronic/steric tunability in comparison with phosphine ligands [37–40]. On the basis of our previous studies on biomimetic chemistry of [FeFe]-hydrogenases [28–30,41–46], we recently initiated a study regarding the synthesis, structures and electrocatalysis of some new NHC-containing model complexes. These model complexes were designed to contain not only the PDT, ADT and ODT (oxadithiolate) cofactors, but also to include a mono-NHC or a di-NHC ligand. The main purposes for such a study are (i) to prepare the first NHC-containing ODT-type model, as well as the other types of new NHC models, and (ii) to examine the influences of different dithiolate cofactors and NHC ligands upon the structures and properties of the synthesized NHC model complexes. As a result, five new NHC ligand-containing models along with one new NHC precursor were synthesized and structurally characterized. In addition, some influences of the dithiolate cofactors and NHC ligands upon the synthesized models, particularly upon their structures and properties, were also observed. Herein, we report these interesting results obtained from this study.

* Corresponding author. Fax: +86 22 23504853.
E-mail address: lcsong@nankai.edu.cn (L.-C. Song).

0022-328X/$ - see front matter © 2008 Published by Elsevier B.V.
doi:10.1016/j.jorganchem.2008.10.015

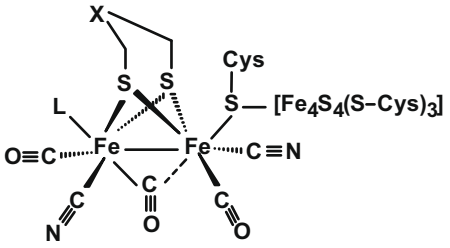

Chart 1. [FeFe]-hydrogenase H-cluster structure. X = CH_2, NH, or O; L = vacant (H_{ox}), H_2O, CO (H_{ox}–CO), H_2 or H.

2. Results and discussion

2.1. Synthesis and characterization of mono-NHC model compounds 1–3 prepared from NHC precursor I_{Mes}·HCl and parent complexes A–C

We found that treatment of diiron all-carbonyl complexes $[(\mu\text{-}SCH_2)_2X]Fe_2(CO)_6$ (**A**, X = O; **B**, X = NBu-*t*; **C**, X = NC_6H_4OMe-*p*) in THF at room temperature with heterocyclic carbene I_{Mes} (generated in situ by reaction of the NHC precursor 1,3-bis(mesityl)imidazolium salt I_{Mes}·HCl with *n*-BuLi or *t*-BuOK [47]) resulted in formation of the corresponding mono-NHC-containing compounds $[(\mu\text{-}SCH_2)_2X]Fe_2(CO)_5(I_{Mes})$ (**1**, X = O; **2**, X = NBu-*t*; **3**, X = NC_6H_4-OMe-*p*) in 50–70% yields (Scheme 1).

Complexes **1**–**3** are air-stable red solids, which have been characterized by elemental analysis and spectroscopy. The ^1H NMR spectra of **1**–**3** displayed a singlet at ca. 7.1 ppm for their imidazole protons and two singlets at ca. 2.18 and ca. 2.35 ppm for methyl protons in their mesityl groups. The ^{13}C NMR spectra of **1**–**3** exhibited a singlet at ca. 190 ppm, which is typical of a carbene carbon atom [32,48]. The IR spectra of **1**–**3** showed three to four absorption bands in the region 2039–1924 cm^{-1} for their terminal carbonyls. The highest frequencies of these $\nu_{C\equiv O}$ bands are shifted by ca. 40 cm^{-1} toward lower values relative to those corresponding to their parent complexes **A** [41], **B** [49] and **C** [30]. This is because *N*-heterocyclic carbene I_{Mes} is a stronger σ-donor (than CO) with negligible π-accepting ability [50].

The molecular structures of **1**–**3** were confirmed by X-ray crystallography. The ORTEP plots are presented in Figs. 1–3 and Tables 1–3 list the selected bond lengths and angles. As shown in Figs. 1–3, the geometric shapes of the Fe_2S_2 skeletons in **1**–**3** are all butterfly-shaped, which were also found in other Fe_2S_2 model complexes [22,26,41]. The cofactors ODT and ADT are bridged between the two iron atoms of $Fe(CO)_3$ and $Fe(CO)_2$ moieties to form two fused six-membered rings Fe1S1C6XC7S2 and Fe2S1C6XC7S2 (X = O6 or N1). The tertiary butyl group in **2** is equatorially attached to the common N1 atom of the two fused six-membered rings, whereas the *p*-$MeOC_6H_4$ group in **3** is axially bound to N1 atom. The NHC ligand I_{Mes} lies in the basal positions of **2** and **3**, but ligands I_{Mes} and L_{Me} (L_{Me} = 1,3-bis(methyl)imidazol-2-ylidene) reside in apical positions of compound **1**, $[(\mu\text{-}SCH_2)_2CH_2]Fe_2(CO)_5(L_{Me})$ [33] and $[(\mu\text{-}SCH_2)_2CH_2]Fe_2(CO)_5(I_{Mes})$ [34], respectively. The basal location of I_{Mes} in **2** and **3** is apparently in order to avoid the strong steric repulsions between the bulky NHC ligand and the N1-attached bulky *t*-Bu and *p*-$MeOC_6H_4$ groups. The Fe1–Fe2 bond lengths of **1** (2.5493 Å), **2** (2.5860 Å), and **3** (2.5525 Å) are much longer than the corresponding bond lengths of parent complexes **A** (2.5113 Å) [41] and **C** (2.5076 Å) [30], but they are very close to the corresponding bond length in the reduced form of DdH hydrogenase (2.55 Å) [12].

2.2. Synthesis and characterization of NHC precursor $[I^*_{Mes}(CH_2)_3I^*_{Mes}]\cdot 2HBr$ prepared from 1-(mesityl)imidazole and $Br(CH_2)_3Br$

The propylene-bridged imidazolium salt $[I^*_{Mes}(CH_2)_3I^*_{Mes}]\cdot 2HBr$ (I^*_{Mes} = 1-(mesityl)imidazol-2-ylidene) could be prepared, similar to the methylene-bridged imidazoium salt [51], by reaction of 1-(mesityl)imidazole with $Br(CH_2)_3Br$ in toluene at reflux in 71% yield (Scheme 2).

Imidazolium salt $[I^*_{Mes}(CH_2)_3I^*_{Mes}]\cdot 2HBr$ is an easily deliquescent white solid, which was characterized by elemental analysis and spectroscopy. For example, its ^1H NMR spectrum displayed a singlet at 9.98 ppm for protons of the two NCHN units in its bridged two imidazole rings, whereas its ^{13}C NMR spectrum showed two singlets at 122.99 and 124.70 ppm for carbon atoms of the two NCH=CHN groups in its bridged imidazole rings.

The molecular structure of this imidazolium salt has been determined by X-ray diffraction analysis. Fig. 4 depicts its ORTEP diagram and Table 4 lists its selected bond lengths and angles. As can be seen in Fig. 4, it consists of two bromide anions and one propylene-bridged bis(mesityl)imidazolium dication. The dihedral angles between mesitylene ring and imidazole ring involving its C1–N1 and C19–N4 bonds are 90.8° and 70.7°, respectively. The C–C and C–N bond lengths are very close to those corresponding to the analogous methyl-substituted imidazolium salt [52].

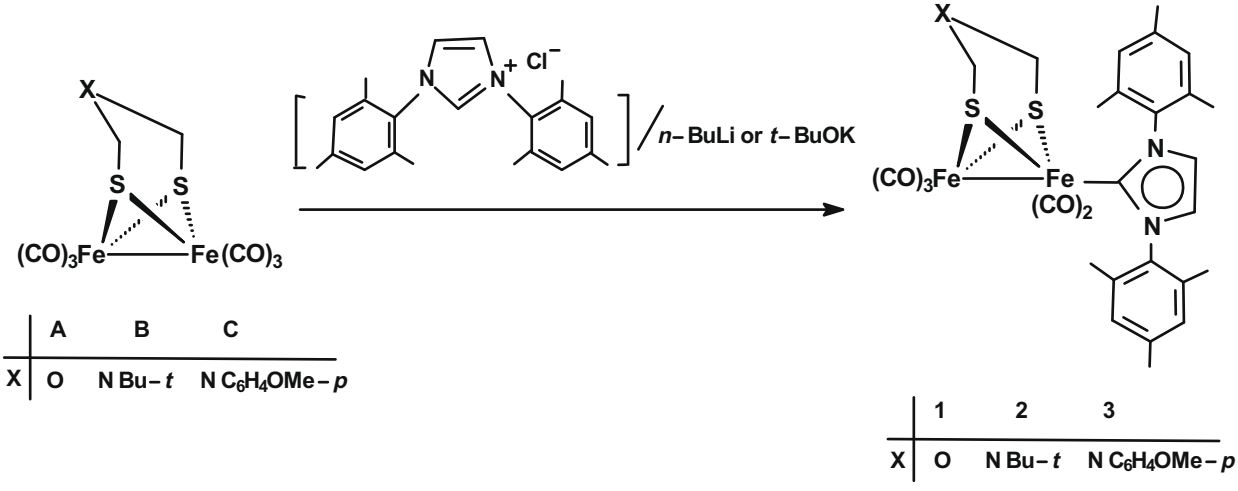

Scheme 1. Synthesis of compounds **1**–**3**.

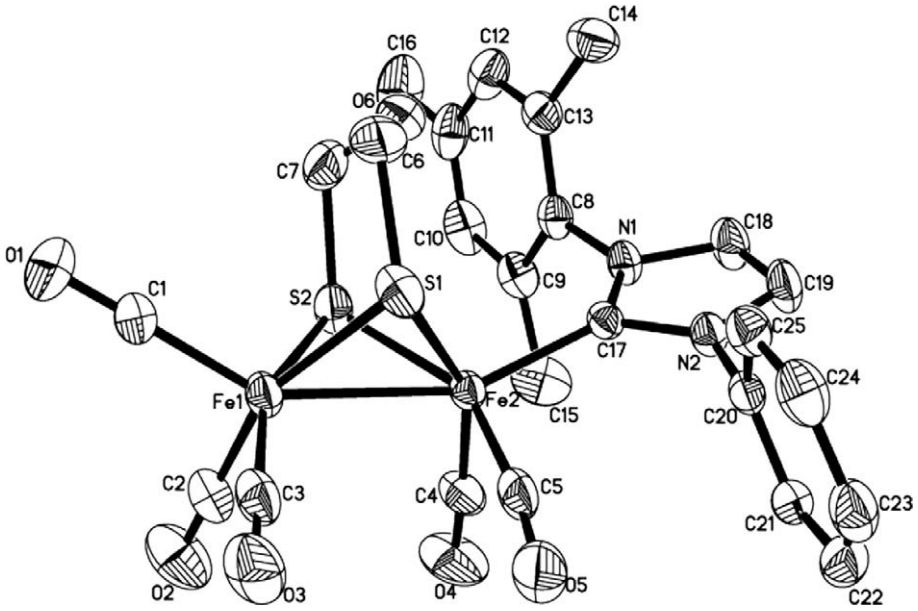

Fig. 1. Molecular structure of **1** with 30% probability level ellipsoids.

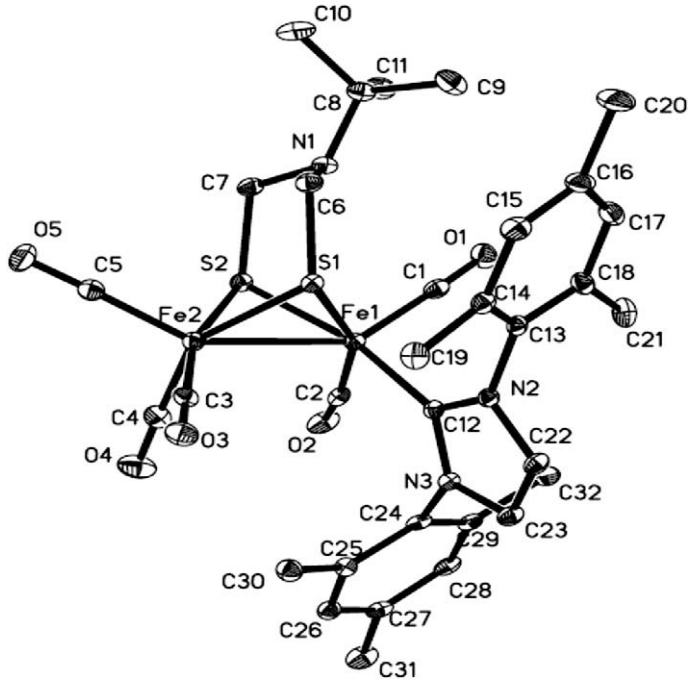

Fig. 2. Molecular structure of **2** with 30% probability level ellipsoids.

*2.3. Synthesis and characterization of mono- and di-NHC model compounds **4** and **5** prepared from NHC precursor [I*Mes(CH2)3I*Mes]·2HBr and parent complexes **B** and **D***

Interestingly, the propylene-bridged imidazolium salt [I*Mes- $(CH_2)_3$I*Mes]·2HBr reacted with *n*-BuLi in THF at room temperature followed by treatment of the resulting mixture with parent compound **B** to give the mono-NHC ligand [I*Mes$(CH_2)_3$I*Mes]·HBr-substituted model compound **4** in 37% yield (Scheme 3). However, in contrast to this, when imidazolium salt [I*Mes$(CH_2)_3$I*Mes]·2HBr reacted with *n*-BuLi followed by treatment of the resulting mixture with parent complex [$(\mu$-$SCH_2)_2$-CH_2]$Fe_2(CO)_6$ (**D**) under similar conditions, the di-NHC ligand I*Mes$(CH_2)_3$I*Mes-substituted model complex [$(\mu$-$SCH_2)_2CH_2Fe_2$-$(CO)_5$]$_2$[μ-I*Mes$(CH_2)_3$I*Mes] (**5**) was produced in 52% yield (Scheme 4). Apparently, these observations demonstrated that (i) the resulting mixture formed from *n*-BuLi and [I*Mes$(CH_2)_3$I*Mes]·2HBr contains not only mono-NHC [I*Mes$(CH_2)_3$I*Mes]·2HBr, but also di-NHC I*Mes$(CH_2)_3$I*Mes, and (ii) the bridged dithiolate cofactors in **B** and **D** play a key role for production of such two types of model complexes.

Both compounds **4** and **5** are air-stable red solids, which have been characterized by elemental analysis and spectroscopy. The ^{1}H NMR spectrum of **4** displayed a singlet at 9.93 ppm, but **5** did not show this signal. This is consistent with the fact that **4** has one imidazole ring with the NCHN group, but **5** does not have

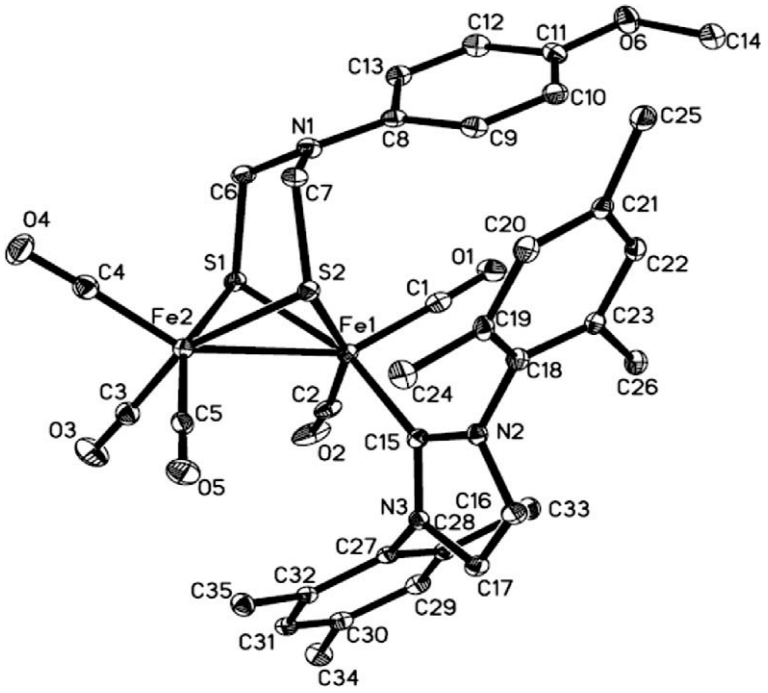

Fig. 3. Molecular structure of **3** with 30% probability level ellipsoids.

Table 1
Selected bond lengths (Å) and angles (°) for **1**.

Bond lengths			
Fe(1)–C(1)	1.782(6)	Fe(1)–S(1)	2.2766(14)
Fe(1)–S(2)	2.2793(15)	Fe(1)–Fe(2)	2.5493(9)
Fe(2)–S(2)	2.2698(14)	N(1)–C(17)	1.385(5)
Fe(2)–C(17)	2.010(4)	O(6)–C(6)	1.420(8)
Bond angles			
S(1)–Fe(2)–Fe(1)	55.99(4)	S(1)–Fe(1)–S(2)	83.78(5)
S(2)–Fe(2)–Fe(1)	56.09(4)	Fe(2)–S(1)–Fe(1)	68.16(4)
S(2)–Fe(2)–S(1)	84.08(6)	Fe(2)–S(2)–Fe(1)	68.17(4)
S(2)–Fe(1)–Fe(2)	55.74(4)	C(7)–O(6)–C(6)	111.8(5)
S(1)–Fe(1)–Fe(2)	55.84(3)	N(2)–C(17)–N(1)	102.6(3)

Table 2
Selected bond lengths (Å) and angles (°) for **2**.

Bond lengths			
Fe(1)–C(12)	2.004(3)	Fe(2)–S(1)	2.2483(8)
Fe(1)–S(1)	2.2443(7)	Fe(2)–S(2)	2.2719(8)
Fe(1)–S(2)	2.2732(8)	N(1)–C(6)	1.446(3)
Fe(1)–Fe(2)	2.5860(6)	N(2)–C(12)	1.384(3)
Bond angles			
S(1)–Fe(1)–S(2)	83.29(3)	S(1)–Fe(2)–Fe(1)	54.79(2)
N(2)–C(12)–N(3)	102.3(2)	C(6)–N(1)–C(7)	109.9(2)
S(2)–Fe(1)–Fe(2)	55.30(2)	Fe(1)–S(1)–Fe(2)	70.29(2)
S(1)–Fe(1)–Fe(2)	54.93(2)	S(2)–Fe(2)–Fe(1)	55.34(2)
S(1)–Fe(2)–S(2)	83.23(3)	Fe(2)–S(2)–Fe(1)	69.36(2)

Table 3
Selected bond lengths (Å) and angles (°) for **3**.

Bond lengths			
Fe(1)–S(2)	2.2251(9)	Fe(1)–Fe(2)	2.5525(6)
Fe(1)–S(1)	2.2501(8)	N(1)–C(7)	1.416(4)
Fe(2)–S(2)	2.2358(8)	N(1)–C(8)	1.407(4)
Fe(2)–S(1)	2.2467(8)	Fe(1)–C(15)	1.994(3)
Bond angles			
S(2)–Fe(1)–S(1)	83.73(3)	Fe(2)–S(1)–Fe(1)	69.17(3)
S(2)–Fe(1)–Fe(2)	55.29(2)	Fe(1)–S(2)–Fe(2)	69.81(3)
S(1)–Fe(1)–Fe(2)	55.35(2)	C(6)–N(1)–C(7)	114.0(2)
S(2)–Fe(2)–S(1)	83.56(3)	N(2)–C(15)–N(3)	102.1(2)
S(2)–Fe(2)–Fe(1)	54.90(2)	S(1)-Fe(2)–Fe(1)	55.48(2)

any NCHN unit. Also consistent with this fact is that the ^{13}C NMR spectrum of **4** exhibited one singlet at 187.26 ppm for the carbene C atom in its N$\ddot{C}$N moiety and **5** displayed two signals at 188.70 and 188.89 ppm for the carbene carbon atoms in its two N$\ddot{C}$N moieties [32,48]. Based on the same reason as indicated above for monocarbene I_{Mes}, the NHC ligands $[I^*_{Mes}(CH_2)_3I^*_{Mes}]\cdot HBr$ and $I^*_{Mes}(CH_2)_3I^*_{Mes}$ can make the highest $\nu_{C\equiv O}$ frequencies of **4** and **5** shift toward lower frequencies by 37 and 39 cm^{-1} relative to the corresponding frequencies of their parent complexes **B** and **D**, respectively [49]. The molecular structures of **4** and **5** were unambiguously confirmed by X-ray diffraction analysis. Figs. 5 and 6 show their ORTEP diagrams, and Tables 5 and 6 present their selected bond lengths and angles. The X-ray crystallography revealed

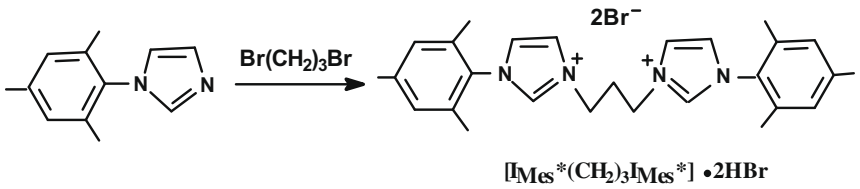

Scheme 2. Synthesis of $[I^*_{Mes}(CH_2)_3I^*_{Mes}]\cdot 2HBr$.

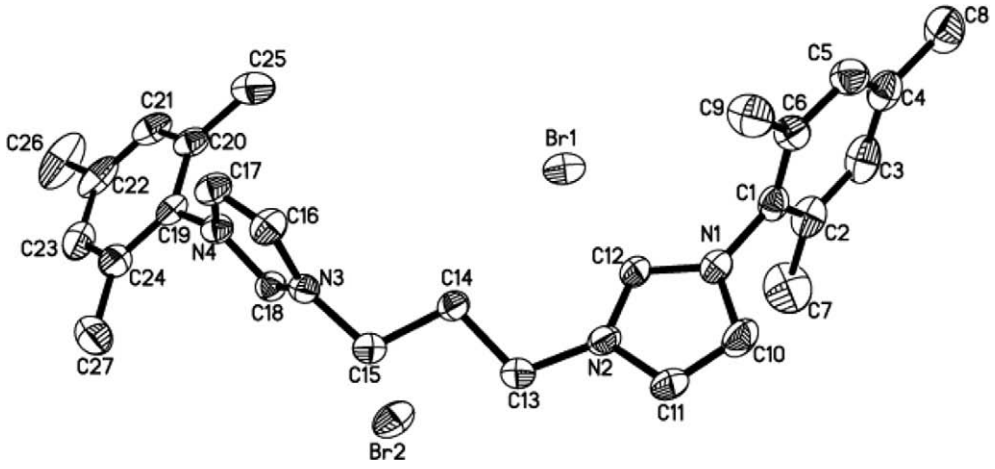

Fig. 4. Molecular structure of $[I^{*}_{Mes}(CH_2)_3I^{*}_{Mes}]\cdot 2HBr$ with 30% probability level ellipsoids.

Table 4
Selected bond lengths (Å) and angles (°) for $[I^{*}_{Mes}(CH_2)_3I^{*}_{Mes}]\cdot 2HBr$.

Bond lengths			
N(1)–C(12)	1.315(6)	N(1)–C(10)	1.397(7)
N(1)–C(1)	1.452(7)	N(2)–C(12)	1.316(6)
N(2)–C(11)	1.371(7)	N(2)–C(13)	1.481(7)
N(3)–C(18)	1.312(6)	N(3)–C(16)	1.382(6)
Bond angles			
C(12)–N(1)–C(10)	107.4(5)	C(12)–N(1)–C(1)	128.3(4)
C(10)–N(1)–C(1)	124.3(5)	C(12)–N(2)–C(11)	108.2(5)
C(12)–N(2)–C(13)	128.2(4)	C(11)–N(2)–C(13)	123.4(4)
C(18)–N(3)–C(16)	108.8(4)	C(18)–N(3)–C(15)	124.8(4)

that compound **4** is indeed the monocarbene $[I^{*}_{Mes}(CH_2)_3I^{*}_{Mes}]\cdot$HBr-substituted diiron ADT model compound, whereas **5** is the dicarbene $I^{*}_{Mes}(CH_2)_3I^{*}_{Mes}$-bridged diiron PDT model complex. The dihedral angles between the mesitylene and imidazole rings involving C20–N1 and C30–N4 bonds in **4** are 84.0° and 95.3°, whereas those involving C12–N1 and C12A–N1A in **5** are all 83.3° due to its plane symmetry. It is interesting to note that the monocarbene in **4** is coordinated to Fe2 with a basal mode, while dicarbene $I^{*}_{Mes}(CH_2)_3I^{*}_{Mes}$ in **5** is coordinated to Fe2 and Fe2A with an apical/apical mode. The latter coordination mode is actually the same as that adopted by the bridged dicarbene $I_{Me}CH_2I_{Me}$ in analogous complex $[(\mu\text{-}SCH_2)_2CH_2Fe_2(CO)_5]_2[\mu\text{-}I^{*}_{Mes}CH_2I^{*}_{Mes}]$ [32]. The Fe1–Fe2 bond lengths of **4** (2.5595 Å) and **5** (2.5390 Å) are slightly shorter than the corresponding bond lengths of **1–3**. In addition, the Fe–C_{NHC} bond lengths of **4** (Fe2–C23 = 1.987 Å) and **5** (Fe2–C18 = 2.003 Å) are very close to the corresponding those of **1** (2.010 Å), **2** (2.004 Å) or **3** (1.994 Å) and the other Fe–C_{NHC} bond lengths in similar model complexes [32–36].

2.4. Electrochemistry of *1* and *2*

The electrochemical properties of **1** and **2** were determined by CV techniques under CO atmosphere, and their electrochemical data are listed in Table 7. It is shown that the first reductions of **1** and **2** (E_{pc} = –1.97 and –2.07 V) are irreversible two-electron processes (confirmed by bulk electrolyses of **1** and **2** at around –2.25 V). The second reductions of **1** and **2** could not be able to obtain because they are beyond the electrochemical window of MeCN. It follows that the first reduction behavior of **1** and **2** under CV conditions is very similar to each other, although they have different dithiolate cofactors.

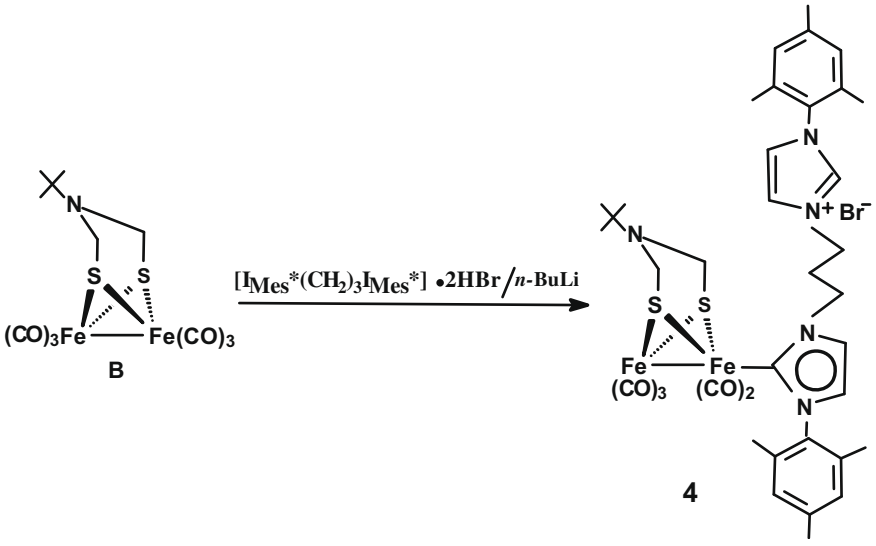

Scheme 3. Synthesis of compound **4**.

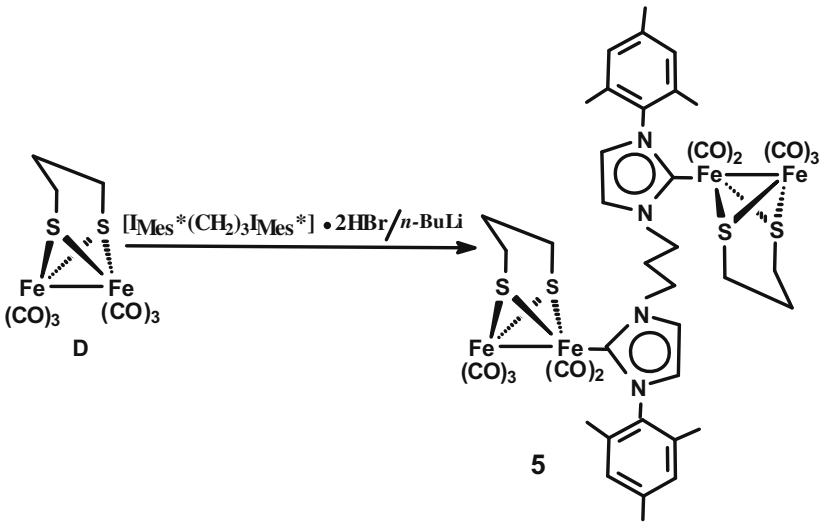

Scheme 4. Synthesis of compound **5**.

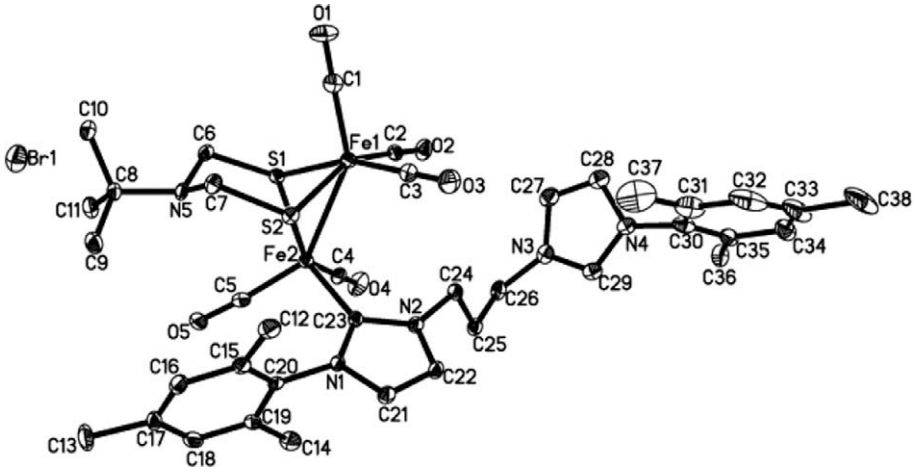

Fig. 5. Molecular structure of **4** with 30% probability level ellipsoids.

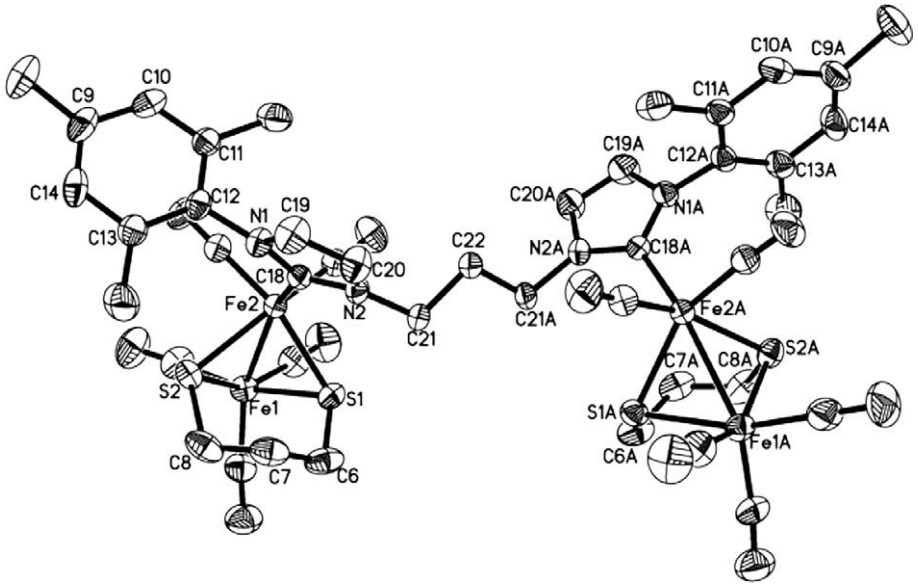

Fig. 6. Molecular structure of **5** with 30% probability level ellipsoids.

Table 5
Selected bond lengths (Å) and angles (°) for **4**.

Bond lengths			
Fe(1)–S(2)	2.2508(13)	S(1)–C(6)	1.839(4)
Fe(1)–S(1)	2.2587(14)	N(2)–C(21)	1.378(5)
Fe(2)-S(2)	2.2365(13)	Fe(1)–Fe(2)	2.5595(10)
Fe(2)–S(1)	2.2417(13)	N(3)–C(27)	1.381(6)
Bond angles			
S(2)–Fe(1)–S(1)	83.61(4)	Fe(2)–S(1)–Fe(1)	69.32(4)
S(2)–Fe(1)–Fe(2)	54.96(4)	Fe(1)–S(2)–Fe(2)	69.55(4)
S(1)–Fe(1)–Fe(2)	55.03(4)	N(2)–C(23)–N(1)	102.5(3)
S(2)–Fe(2)–S(1)	84.32(4)	C(7)–N(5)–C(6)	109.7(4)
S(2)–Fe(2)–Fe(1)	55.49(3)	N(1)–C(23)–Fe(2)	128.0(3)

Table 6
Selected bond lengths (Å) and angles (°) for **5**.

Bond lengths			
Fe(1)–S(2)	2.2679(18)	S(1)–C(6)	1.822(7)
Fe(1)–S(1)	2.2554(18)	N(2)–C(21)	1.457(6)
Fe(2)-S(2)	2.2825(18)	Fe(1)–Fe(2)	2.5390(16)
Fe(2)–S(1)	2.265(2)	Fe(2)–C(18)	2.003(5)
Bond angles			
S(2)–Fe(1)–S(1)	85.08(7)	Fe(2)-S(1)–Fe(1)	68.34(5)
S(2)–Fe(1)–Fe(2)	56.36(5)	Fe(1)–S(2)–Fe(2)	67.83(5)
S(1)–Fe(1)–Fe(2)	56.01(5)	N(1)–C(18)–N(2)	103.1(4)
S(2)–Fe(2)–S(1)	84.51(8)	C(6)–C(7)–C(8)	113.3(6)
S(2)–Fe(2)–Fe(1)	55.81(5)	Fe(2)–C(18)–N(2)	129.0(4)

Table 7
Redox potentials of **1** and **2**[a].

Compound	E_{pc}/V	E_{pa}/V
1	−1.97	+0.13
2	−2.07	+0.01

[a] All potentials are versus Fc/Fc^+ in 0.1 M $^nBu_4NPF_6$/MeCN at a scan rate of 100 mV s^{-1}.

In order to examine whether such NHC-containing compounds possess electrocatalytic ability for proton reduction to hydrogen, we further determined the electrochemical properties of **2** in the presence of HOAc and without HOAc (for comparative purpose). As shown in Fig. 7, when HOAc was sequentially added from 2 mM to 10 mM, the initial peak at −2.07 V (in the absence of HOAc) obviously grew up, which is typical of an electrocatalytic process [53–57]. To further confirm this, we carried out bulk electrolysis of a MeCN solution containing HOAc (25 mM) and **2** (0.5 mM) at −2.40 V. During 0.5 h of this bulk electrolysis, 17.2 F per mole of **2** passed, which corresponds to 8.6 turnovers. Gas chromatography showed that the hydrogen yield is >90%.

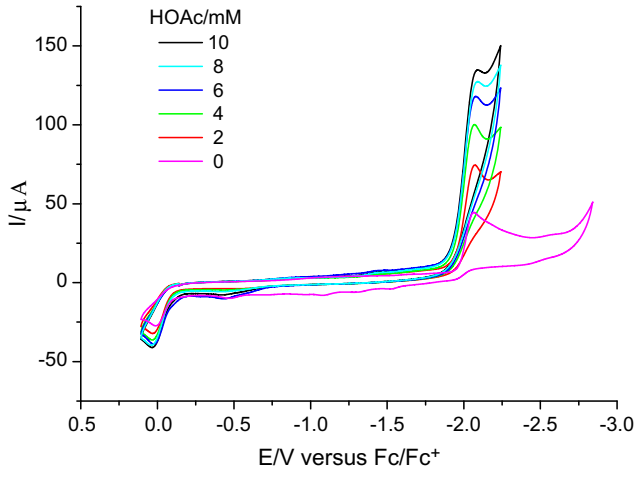

Fig. 7. Cyclic voltammograms of **2** (1.0 mM) with HOAc (0–10 mM) in 0.1 M *n*-Bu_4NPF_6/MeCN at a scan rate of 100 mV s^{-1}.

On the basis of the aforementioned experimental observations and the previously reported similar cases [41–43,53–56], we might propose an EECC (E = electrochemical, C = chemical) mechanism to account for this electrochemical process catalyzed by **2** (Scheme 5). First, complex **2** accepts two electrons at the same potential (−2.07 V) by the Fe atom without I_{Mes} ligand and the I_{Mes} ligand attached to Fe atom, which results in formation of dianion $\mathbf{2}^{2-}$. Then, the Fe atom without I_{Mes} ligand in the electron-rich dianion $\mathbf{2}^{2-}$ is protonated to afford the Fe–H species of monoanion $\mathbf{2H}^-$. The Fe atom with I_{Mes} ligand in $\mathbf{2H}^-$ is further protonated and followed by intramolecular electron transfer from the reduced I_{Mes} ligand to its attached Fe atom to regenerate catalyst **2** with evolution of hydrogen. Actually, this mechanism is very similar to that proposed for H_2 evolution catalyzed by the cofacial bisorganometallic Ru and Os diporphyrins [58], as well as by the NHC ligand-containing diiron PDT compound [34].

3. Experimental section

All reactions were carried out using standard Schlenk and vacuum-line techniques under an atmosphere of nitrogen. THF and toluene were purified by distillation from sodium/benzophenone ketyl. While 1,3-bis(mesityl)imidazolium chloride [59], $[(\mu\text{-}SCH_2)_2O]Fe_2(CO)_6$ [41], $[(\mu\text{-}SCH_2)_2NBu\text{-}t]Fe_2(CO)_6$ [60], $[(\mu\text{-}SCH_2)_2NC_6H_4OMe\text{-}p]Fe_2(CO)_6$ [30], $[(\mu\text{-}SCH_2)_2CH_2]Fe_2(CO)_6$ [61], and 1-(mesityl)imidazole [52] were prepared according to the published methods, the other starting materials were commercially available and used without further purification. IR spectra were recorded on a Bio-Rad FTS 6000 infrared spectrophotometer. ^1H and ^{13}C NMR spectra were taken on a Bruker Avance 300 NMR or a Varian Mercury Plus 400 NMR spectrometer. Elemental analyses were performed on an Elementar Vario EL analyzer. Melting points were determined on a Yanaco MP-500 apparatus and are uncorrected.

3.1. Synthesis of $[(\mu\text{-}SCH_2)_2O]Fe_2(CO)_5(I_{Mes})$ (**1**)

To a stirred suspension of 0.300 g (0.88 mmol) of 1,3-bis(mesityl)imidazolium salt I_{Mes}·HCl in THF (15 mL) was slowly added 0.4 mL (1.00 mmol) of *n*-BuLi (2.5 M in hexane) to give a yellowish solution. After stirring at room temperature for additional 10 min, the reaction mixture was filtered under anaerobic conditions through a Celite-packed column and eluted with THF (10 mL) to give a filtrate containing the air-sensitive free carbene I_{Mes}. To the filtrate was added 0.077 g (0.20 mmol) of $[(\mu\text{-}SCH_2)_2O]Fe_2(CO)_6$ (**A**) and the new mixture was stirred at room temperature for 3 h until complete consumption of **A** as indicated by TLC. The resulting deep red solution was evaporated to dryness under vacuum, leaving a brown-red residue which was subjected to TLC separation using acetone/petroleum ether (1:5) as eluent. From the main band was obtained **1** as a dark-red solid (0.093 g, 70%), m.p. 165 °C (dec. in a sealed capillary). Anal. Calc. for $C_{28}H_{28}Fe_2N_2O_6S_2$: C, 50.62; H, 4.25; N, 4.22. Found: C, 50.53; H, 4.19; N, 4.49%. IR (KBr disk): $\nu_{C\equiv O}$ 2039vs, 1969vs, 1947s, 1924s cm^{-1}. ^1H NMR (400 MHz, $CDCl_3$): δ 2.17 (s, 12H, 4*o*-ArCH_3), 2.34 (s, 6H, 2*p*-ArCH_3), 3.66 (s, 4H, CH_2OCH_2), 7.00 (s, 4H, 4*m*-Ar*H*), 7.14 (s, 2H, NCH=CHN). ^{13}C NMR (75.4 MHz, $CDCl_3$): δ 18.46 (s, *o*-ArCH_3), 21.10 (s, *p*-ArCH_3), 68.53 (s, CH_2OCH_2), 124.83 (s, NCH=CHN), 129.16, 136.29, 137.85, 139.23 (4s, C_6H_2), 190.44 (s, NCN), 209.83, 214.04 (2s, C≡O).

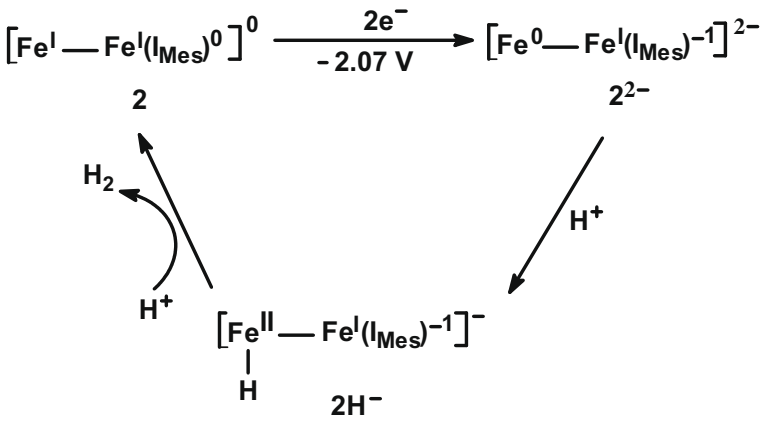

Scheme 5. The EECC mechanism for the electrocatalytic proton reduction catalyzed by **2**.

3.2. Synthesis of [(μ-SCH_2)$_2$NBu-t]$Fe_2(CO)_5(I_{Mes})$ (**2**)

To the above-prepared filtrate containing free carbene I_{Mes} was added 0.090 g (0.20 mmol) of [(μ-SCH_2)$_2$NBu-*t*]$Fe_2(CO)_6$ (**B**). The mixture was stirred at room temperature for 3 h until **B** was disappeared as indicated by TLC. After removal of the volatiles under vacuum, the residue was subjected to TLC separation using THF/petroleum ether (1:15) as eluent. From the main band was obtained **2** as a purple-red solid (0.076 g, 53%), m.p. 105 °C (dec. in a sealed capillary). Anal. Calc. for $C_{32}H_{37}Fe_2N_3O_5S_2$: C, 53.42; H, 5.18; N, 5.84. Found: C, 53.18; H, 5.10; N, 5.60%. IR (KBr disk): $\nu_{C\equiv O}$ 2026s, 1973vs, 1939vs cm^{-1}. ^1H NMR (300 MHz, $CDCl_3$): δ 0.84 (s, 9H, C(CH_3)$_3$), 2.20 (s, 12H, 4*o*-ArCH_3), 2.34 (s, 6H, 2*p*-ArCH_3), 2.93, 2.96 (2s, 4H, CH_2NCH_2), 7.00 (s, 4H, 4*m*-Ar*H*), 7.03 (s, 2H, NCH=CHN). ^{13}C NMR (75.4 MHz, $CDCl_3$): δ 18.61 (s, *o*-ArCH_3), 21.06 (s, *p*-ArCH_3), 26.22 (s, C(CH_3)$_3$), 46.71 (s, CH_2NCH_2), 56.59 (s, *C*(CH_3)$_3$), 124.77 (s, NCH=CHN), 129.22, 136.27, 137.81, 139.04 (4s, C_6H_2), 190.95 (s, NCN), 211.59, 214.46 (2s, C≡O).

3.3. Synthesis of [(μ-SCH_2)$_2$$NC_6H_4$OMe-p]$Fe_2(CO)_5(I_{Mes})$ (**3**)

Method A. To the above-prepared filtrate containing free carbene I_{Mes} was added 0.100 g (0.20 mmol) of [(μ-SCH_2)$_2$$NC_6H_4$OMe-*p*]$Fe_2(CO)_6$ (**C**). The mixture was stirred at room temperature for 5 h until **C** was completely consumed. Solvent was removed under vacuum and the residue was subjected to TLC separation using CH_2Cl_2/petroleum ether (1:5) as eluent. From the main band was obtained **3** as a dark-red solid (0.091 g, 59%), m.p. 152 °C (dec. in a sealed capillary). Anal. Calc. for $C_{35}H_{35}Fe_2N_3O_6S_2$: C, 54.63; H, 4.58; N, 5.46. Found: C, 54.44; H, 4.50; N 5.45%. IR (KBr disk): $\nu_{C\equiv O}$ 2027s, 1976vs, 1960vs, 1937s cm^{-1}. ^1H NMR (300 MHz, $CDCl_3$): δ 2.20 (s, 12H, 4*o*-ArCH_3), 2.36 (s, 6H, 2*p*-ArCH_3), 3.16, 3.19, 3.70 (3s, 4H, CH_2NCH_2), 3.75 (s, 3H, CH_3O), 6.49, 6.52, 6.76, 6.79 (AB quartet, 4H, C_6H_4), 7.03 (s, 4H, 4*m*-Ar*H*), 7.05 (s, 2H, NCH=CHN). ^{13}C NMR (75.4 MHz, $CDCl_3$): δ 18.61 (s, *o*-ArCH_3), 21.08 (s, *p*-ArCH_3), 49.10 (s, CH_2NCH_2), 55.67 (s, CH_3O), 125.02 (s, NCH=CHN), 114.64, 117.68, 129.27, 136.29, 137.76, 139.29, 142.34, 153.38 (8s, C_6H_2, C_6H_4), 189.96 (s, NCN), 210.67, 213.93 (2s, C≡O).

Method B. To a stirred suspension of 0.500 g (1.47 mmol) of the imidazolium salt I_{Mes}·HCl in THF (15 mL) was added 0.330 g (2.94 mmol) of *t*-BuOK to give a light yellow solution. After stirring at room temperature for additional 1 h, the mixture was filtered under anaerobic conditions through a Celite-packed column and eluted with THF (15 mL) to give a filtrate containing free carbene I_{Mes}. To the combined filtrate was added 0.110 g (0.22 mmol) of [(μ-SCH_2)$_2$$NC_6H_4$OMe-*p*]$Fe_2(CO)_6$ (**C**) and then the mixture was stirred at room temperature for 6 h until complete consumption of **C.** The same work-up as that described in Method A afforded **3** (0.085 g, 50%).

3.4. Synthesis of [$I^*_{Mes}(CH_2)_3$ I^*_{Mes}]·2HBr

While stirring, a solution of 2.014 g (10.83 mmol) of 1-(mesityl)imidazole and 1.584 g (7.84 mmol) of $Br(CH_2)_3Br$ in toluene (40 mL) was refluxed for about 12 h. During this period of time, white powders were gradually produced. After the mixture had been cooled to room temperature, it was subjected to centrifugal separation. The separated precipitate was thoroughly washed with THF (15 × 4 mL) and dried under vacuum to give **4** as a white solid (2.193 g, 71%), m.p. 281–282 °C (in air). Anal. Calc. for $C_{27}H_{34}N_4Br_2$: C, 56.46; H, 5.97; N, 9.75. Found: C, 56.19; H, 6.07; N, 9.51%. IR (KBr disk): *v* 3057vs, 2969vs, 1554vs, 1487m, 1457s, 1207vs, 1160m, 863s, 773m, 670m cm^{-1}. ^1H NMR (300 MHz, $CDCl_3$): δ 2.07 (s, 12H, 4*o*-ArCH_3), 2.35 (s, 6H, 2*p*-ArCH_3), 3.23 (s, 2H, $CH_2CH_2CH_2$), 4.99 (s, 4H, $CH_2CH_2CH_2$), 7.01 (s, 4H, 4*m*-Ar*H*), 7.11, 8.53 (2s, 4H, 2NCH=CHN), 9.98 (s, 2H, 2NCHN). ^{13}C NMR (75.4 MHz, $CDCl_3$): δ 17.65 (s, *o*-ArCH_3), 21.02 (s, *p*-ArCH_3), 31.80 (s, $CH_2CH_2CH_2$), 47.09 (s, $CH_2CH_2CH_2$), 122.99, 124.70 (2s, NCH=CHN), 129.83, 130.58, 134.14, 141.32, 137.23 (5s, C_6H_2, NCHN).

3.5. Synthesis of [(μ-SCH_2)$_2$NBu-t]$Fe_2(CO)_5$[$I^*_{Mes}(CH_2)_3I^*_{Mes}$] · HBr (**4**)

To a stirred white suspension of 0.300 g (0.52 mmol) of [$I^*_{Mes}(CH_2)_3I^*_{Mes}$]·2HBr in THF (15 mL) at room temperature was dropwise added 0.5 mL (1.25 mmol) of *n*-BuLi (2.5 M in hexane) to give an orange-red solution. After stirring for 15 min, the mixture was filtered under anaerobic conditions through a Celite-packed column and eluted with THF (10 mL) to give a red filtrate. To the filtrate containing the air-sensitive monocarbene [$I^*_{Mes}(CH_2)_3I^*_{Mes}$]·HBr was added 0.06 g (0.14 mmol) of [(μ-SCH_2)$_2$NBu-*t*]$Fe_2(CO)_6$ (**B**) and the new mixture was stirred at room temperature for 5 h until **B** was complete disappeared as indicated by TLC. The resulting mixture was subjected to TLC separation using acetone/petroleum ether (2:1) as eluent. From the main band was obtained **4** as a red solid (0.047 g, 37%), m.p. 159–160 °C (dec. in a sealed capillary). Anal. Calc. for $C_{38}H_{46}BrFe_2N_5O_5S_2$: C, 50.24; H, 5.10; N, 7.71. Found: C, 50.00; H, 5.20; N, 7.47%. IR (KBr disk): $\nu_{C\equiv O}$ 2030vs, 1970vs, 1910s cm^{-1}. ^1H NMR (300 MHz, $CDCl_3$): δ 0.85 (s, 9H, C(CH_3)$_3$), 2.06, 2.11(2s, 12H, 4*o*-ArCH_3), 2.34, 2.35 (2s, 6H, 2*p*-ArCH_3), 2.89, 2.97 (2br.s, 6H, 2NCH_2S, $CH_2CH_2CH_2$), 4.65 (br.s, 4H, N$CH_2CH_2CH_2$N), 6.85, 7.13, 7.51, 7.54 (4s, 4H, 2NCH=CHN), 7.00, 7.02 (2s, 4H, 4*m*-ArH), 9.93 (s, 1H,

NCHN). ^{13}C NMR (75.4 MHz, $CDCl_3$): δ 18.29, 19.05 (2s, *o*-ArCH_3), 21.27 (s, *p*-ArCH_3), 26.37 (s, C(CH_3)$_3$), 33.09 (s, $CH_2CH_2CH_2$), 48.51, 48.61, 48.77 (3s, 2NCH_2, 2NCH_2S), 57.01 (s, *C*(CH_3)$_3$), 123.71, 123.77, 124.16, 125.05 (4s, 2NCH=CHN), 129.34, 130.11, 130.80, 134.39, 136.50, 137.46, 138.37, 139.01, 141.56 (9s, C_6H_2, NCHN), 187.26 (s, NCN), 213.28, 216.39 (2s, C≡O).

3.6. Synthesis of [(μ-SCH$_2$)$_2$CH$_2$Fe$_2$(CO)$_5$][μ-I$^*_{Mes}$(CH$_2$)$_3$I$^*_{Mes}$] (**5**)

To a stirred suspension of 0.650 g (1.14 mmol) of [I$^*_{Mes}$(CH$_2$)$_3$I$^*_{Mes}$]·2HBr in THF (20 mL) at room temperature was dropwise added 1.1 mL (2.75 mmol) of *n*-BuLi to give an orange-red solution. After stirring for 45 min, the mixture was filtered under anaerobic conditions through a Celite-packed column and eluted with THF (15 mL) to give a filtrate. To the filtrate containing the air-sensitive free dicarbene I$^*_{Mes}$(CH$_2$)$_3$I$^*_{Mes}$ was added 0.120 g (0.31 mmol) of [(μ-SCH$_2$)$_2$CH$_2$]Fe$_2$(CO)$_6$ (**D**) and the new mixture was stirred at room temperature for 6 h until **D** was complete disappeared as indicated by TLC. The resulting mixture was subjected to TLC separation using CH_2Cl_2/petroleum ether (5:2) as eluent. From the main band was obtained **5** as a red solid (0.091 g, 52%), m.p. 164 °C (dec. in a sealed capillary). Anal. Calc. for $C_{43}H_{44}Fe_4N_4O_{10}S_4$: C, 45.77; H, 3.93; N, 4.96. Found: C, 45.70; H, 4.02; N, 4.71%. IR (KBr disk): $\nu_{C\equiv O}$ 2032vs, 1961vs, 1910s, 1897s cm^{-1}. ^{1}H NMR (300 MHz, $CDCl_3$): δ 1.62–1.91 (m, 14H, NCH$_2$*CH$_2$*CH$_2$N, 2S*CH$_2$*CH$_2$*CH$_2$*S), 2.11 (s, 12H, 4*o*-ArC*H$_3$*), 2.36 (s, 6H, 2*p*-ArC*H$_3$*), 4.71- 4.96 (m, 4H, NC*H$_2$*CH$_2$*C*H$_2$*N), 7.02 (s, 4H, 4*m*-Ar*H*), 6.91, 7.17 (2s, 4H, 2NCH=CHN). ^{13}C NMR (75.4 MHz, $CDCl_3$): δ 18.55 (s, *o*-ArCH_3), 21.14 (s, *p*-ArCH_3), 25.69, 30.33, 31.91, 33.91 (4s, S$CH_2CH_2CH_2$S, N$CH_2CH_2CH_2$N), 48.80 (N$CH_2CH_2CH_2$N), 122.07, 124.91 (2s, NCH CHN), 129.25, 136.21, 137.23, 139.11(4s, C_6H_2), 188.70, 188.89 (2s, NCN), 207.69, 211.01, 215.90 (3s, C≡O).

3.7. X-ray structure determinations of **1–5** and [I$^*_{Mes}$(CH$_2$)$_3$I$^*_{Mes}$]·2HBr

Single-crystals of **1–5** and [I$^*_{Mes}$(CH$_2$)$_3$I$^*_{Mes}$]·2HBr suitable for X-ray diffraction analyses were grown by slow evaporation of their $CHCl_3$ or CH_2Cl_2/hexane solutions at about −10 °C. A single-crystal of **2–5** was mounted on a Rigaku MM-007 (rotating anode) diffractometer equipped with Saturn 70CCD. Data were collected at 113 K for **2** and **3**, and at 293 K for **4** and **5** using a confocal monochromator with Mo Kα radiation (0.71070 Å) in the $\omega-\varphi$ scanning mode. Data collection, reduction and absorption correction were performed by CRYSTALCLEAR program [62]. A single-crystal of **1** or [I$^*_{Mes}$(CH$_2$)$_3$ I$^*_{Mes}$]·2HBr was mounted on a Bruker SMART 1000 diffractometer. Data were collected at 293 K by using a graphite monochromator with Mo kα radiation (0.71073 Å) in the $\omega-\varphi$ scanning mode. Absorption correction was performed by SADABS program [63]. All the structures were solved by direct methods using the SHELXS-97 program [64] and refined by full-matrix least-squares techniques (SHELXL-97) [65] on F^2. Hydrogen atoms were located using the geometric method. Details of crystal data, data collections, and structure refinement are summarized in Tables 8 and 9.

3.8. Electrochemistry

Acetonitrile (HPLC grade) was used for electrochemistry assays. A solution of 0.1 M *n*-Bu_4NPF_6 in MeCN was used as electrolyte in all cyclic voltammetric experiments. Electrochemical measurements were made using a BAS Epsilon potentiostat. All voltammograms were obtained in a three-electrode cell with a 3 mm diameter glassy carbon working electrode, a platinum counter electrode, and an Ag/Ag$^+$ (0.01 M $AgNO_3$/0.1 M *n*-Bu_4NPF_6 in MeCN) reference electrode under CO atmosphere. The working electrode was polished with 0.05 μm alumina paste and sonicated in water for 10 min prior to use. Bulk electrolysis was run on a vitreous carbon rod (ca. 3 cm^2) in a two-compartment, gastight, H-type electrolysis cell containing ca. 20 mL of MeCN. All potentials are quoted against the ferrocene/ferrocenium (Fc/Fc$^+$) potential. Gas chromatography was performed with a Shimadzu gas chro-

Table 8
Crystal data and structure refinement details for **1**, **2** and **3**.

	1	**2**	**3**
Formula	$C_{28}H_{28}Fe_2N_2O_6S_2$	$C_{32}H_{37}Fe_2N_3O_5S_2$	$C_{35}H_{35}Fe_2N_3O_6S_2$
Formula weight	664.34	719.47	769.48
Crystal system	Triclinic	Orthorhombic	Monoclinic
Space group	*P*$\bar{1}$	*P 21 21 21*	*P 1 21/n 1*
a (Å)	11.596(3)	10.0830(12)	9.6836(7)
b (Å)	16.877(5)	10.3191(12)	14.2893(12)
c (Å)	17.250(5)	31.768(4)	23.7325(17)
α (°)	97.272(5)	90	90
β (°)	106.852(4)	90	90.119(3)
γ (°)	103.165(5)	90	90
V (Å^3)	3078.2(15)	3305.4(7)	3283.9(4)
Z	4	4	4
D_{calc} (g cm^{-3})	1.434	1.446	1.556
μ (Mo Kα) (mm^{-1})	1.120	1.048	1.062
F(000)	1368	1496	1592
Limiting indices	$-13 \leqslant h \leqslant 13$ $-20 \leqslant k \leqslant 12$ $-20 \leqslant l \leqslant 20$	$-13 \leqslant h \leqslant 13$ $-13 \leqslant k \leqslant 13$ $-41 \leqslant l \leqslant 40$	$-12 \leqslant h \leqslant 12$ $-18 \leqslant k \leqslant 18$ $-31 \leqslant l \leqslant 31$
$2\theta_{max}$ (°)	50.04	55.76	55.84
Number of reflections	16016	29597	30750
Number of independent reflections	10791	7871	7842
R	0.0489	0.0398	0.0541
Rw	0.1162	0.0779	0.1013
Goodness of fit	1.032	1.057	1.121
Largest difference in peak and hole (e Å^{-3})	0.657 and −0.533	0.416 and −0.380	0.444 and −0.488

Table 9
Crystal data and structure refinement details for [I$^*_{Mes}$(CH$_2$)$_3$I$^*_{Mes}$]·2HBr, **4** and **5**.

	[I$^*_{Mes}$(CH$_2$)$_3$I$^*_{Mes}$]·2HBr	**4**	**5**
Formula	$C_{27}H_{34}Br_2N_4 \cdot CHCl_3 \cdot 2H_2O$	$C_{38}H_{46}BrFe_2N_5O_5S_2 \cdot 2CHCl_3$	$C_{43}H_{44}Fe_4N_4O_{10}S_4$
Formula weight	729.8	1147.3	1128.5
Crystal system	Monoclinic	Triclinic	Orthorhombic
Space group	*P2(1)/c*	*P*$\bar{1}$	*I b a 2*
a (Å)	15.683(5)	9.467(3)	32.33(2)
b (Å)	7.036(2)	15.787(5)	8.454(5)
c (Å)	31.463(10)	18.766(5)	20.068(12)
α (°)	90	108.379(2)	90
β (°)	98.016(6)	93.365(3)	90
γ (°)	90	105.914(4)	90
V (Å^3)	3437.8(19)	2527.3(12)	5485(6)
Z	4	2	4
D_{calc} (g cm^{-3})	1.41	1.508	1.366
μ (Mo Kα) (mm^{-1})	2.621	1.809	1.241
F(000)	1488	1168	2312
Limiting indices	$-19 \leqslant h \leqslant 18$ $-8 \leqslant k \leqslant 7$ $-30 \leqslant l \leqslant 39$	$-11 \leqslant h \leqslant 11$ $-18 \leqslant k \leqslant 18$ $-22 \leqslant l \leqslant 22$	$-42 \leqslant h \leqslant 42$ $-11 \leqslant k \leqslant 10$ $-26 \leqslant l \leqslant 25$
$2\theta_{max}$ (°)	53.00	50.02	55.58
Number of reflections	18986	26113	24552
Number of independent reflections	7018	8902	6367
R	0.0603	0.0578	0.0561
Rw	0.1521	0.1229	0.1609
Goodness of fit	1.018	1.081	1.090
Largest difference in peak and hole (e Å^{-3})	1.491 and −0.750	0.807 and −0.781	0.827 and −0.382

matograph GC-9A under isothermal conditions with nitrogen as a carrier gas and a thermal conductivity detector.

4. Conclusion

We have successfully synthesized and characterized the first NHC-containing ODT-type model **1** and the new NHC-containing ADT-type and PDT-type models **2–5**. While models **1–3** all contain a mono-NHC ligand IMes, models **4** and **5** contain a mono-NHC ligand $[I^*_{Mes}(CH_2)_3I^*_{Mes}] \cdot HBr$ and a di-NHC ligand $[I^*_{Mes}(CH_2)_3I^*_{Mes}]$, respectively. The formation of **4** and **5** through reactions of **B** and **D** with the same NHC precursor $[I^*_{Mes}(CH_2)_3I^*_{Mes}]\cdot 2HBr$ reflects the different influences of PDT and *N*-substituted ADT cofactors. The X-ray crystallographic studies have revealed that the NHC ligands I_{Mes} and $I^*_{Mes}(CH_2)_3I^*_{Mes}$ in **1** and **5** lie in an apical position, whereas ligands I_{Mes} and $[I^*_{Mes}(CH_2)_3I^*_{Mes}] \cdot HBr$ in **2–4** are in a basal position. This is probably in order to avoid the strong steric repulsions of the NHC ligands in **2–4** with the bulky *t*-Bu and *p*-$MeOC_6H_4$ groups attached to their bridgehead N atoms. As a representative of the five synthesized NHC models, we have found model **2** to be an electrocatalyst for reduction of HOAc proton to hydrogen. In addition, an EECC mechanism involving the uptake of two electrons at the same reduction potential is briefly suggested for this electrocatalytic H_2 production. Further studies on this mechanism and the designed synthesis of the other NHC-containing model complexes with the improved catalytic function are in progress in this laboratory.

5. Supplementary material

CCDC 667950 for **1**, 667951 for **2**, 667952 for **3**, 696353 for **4**, 667954 for **5** and 667953 for $[I^*_{Mes}(CH_2)_3\ I^*_{Mes}]\cdot 2HBr$ contain the supplementary crystallographic data for this paper. These data can be obtained free of charge from The Cambridge Crystallographic Data Centre via www.ccdc.cam.ac.uk/data_request/cif.

Acknowledgements

We are grateful to the National Natural Science Foundation of China and the Research Fund for the Doctoral Program of Higher Education of China for financial support.

References

[1] R. Cammack, Nature 397 (1999) 214.
[2] M.W.W. Adams, E.I. Stiefel, Science 282 (1998) 1842.
[3] F.A. Armstrong, Curr. Opin. Chem. Biol. 8 (2004) 133.
[4] M.W.W. Adams, E.I. Stiefel, Curr. Opin. Chem. Biol. 4 (2000) 214.
[5] S. Shima, R.K. Thauer, Chem. Rec. 7 (2007) 37.
[6] M. Frey, ChemBiochem 3 (2002) 153.
[7] J. Alper, Science 299 (2003) 1686.
[8] M.Y. Darensbourg, E.J. Lyon, J.J. Smee, Coord. Chem. Rev. 206–207 (2000) 533.
[9] D.J. Evans, C.J. Pickett, Chem. Soc. Rev. 32 (2003) 268.
[10] J.W. Peters, W.N. Lanzilotta, B.J. Lemon, L.C. Seefeldt, Science 282 (1998) 1853.
[11] Y. Nicolet, C. Piras, P. Legrand, C.E. Hatchikian, J.C. Fontecilla-Camps, Structure 7 (1999) 13.
[12] Y. Nicolet, A.L. De Lacey, X. Vernède, V.M. Fernandez, E.C. Hatchikian, J.C. Fontecilla-Camps, J. Am. Chem. Soc. 123 (2001) 1596.
[13] B.J. Lemon, J.W. Peters, Biochemistry 38 (1999) 12969.
[14] A.J. Pierik, M. Hulstein, W.R. Hagen, S.P. Albracht, Eur. J. Biochem. 258 (1998) 572.
[15] A.L. De Lacey, C. Stadler, C. Cavazza, E.C. Hatchikian, V.M. Fernandez, J. Am. Chem. Soc. 122 (2000) 11232.
[16] Z. Chen, B.J. Lemon, S. Huang, D.J. Swartz, J.W. Peters, K.A. Bagley, Biochemistry 41 (2002) 2036.
[17] F. Gloaguen, J.D. Lawrence, M. Schmidt, S.R. Wilson, T.B. Rauchfuss, J. Am. Chem. Soc. 123 (2001) 12518.
[18] E.J. Lyon, I.P. Georgakaki, J.H. Reibenspies, M.Y. Darensbourg, J. Am. Chem. Soc. 123 (2001) 3268.
[19] M. Razavet, S.C. Davies, D.L. Hughes, J.E. Barclay, D.J. Evans, S.A. Fairhurst, X. Liu, C.J. Pickett, Dalton Trans. (2003) 586.
[20] C. Tard, X. Liu, S.K. Ibrahim, M. Bruschi, L. De Giola, S.C. Davies, X. Yang, L.-S. Wang, G. Sawers, C.J. Pickett, Nature 433 (2005) 610.
[21] L.-C. Song, J. Cheng, J. Yan, H.-T. Wang, X.-F. Liu, Q.-M. Hu, Organometallics 25 (2006) 1544.
[22] E.J. Lyon, I.P. Georgakaki, J.H. Reibenspies, M.Y. Darensbourg, Angew. Chem., Int. Ed. 38 (1999) 3178.
[23] J.L. Nehring, D.M. Heinekey, Inorg. Chem. 42 (2003) 4288.
[24] F.I. Adam, G. Hogarth, I. Richards, J. Organomet. Chem. 692 (2007) 3957.
[25] G. Eilers, L. Schwartz, M. Stein, G. Zampella, L. de Gioia, S. Ott, R. Lomoth, Chem. Eur. J. 13 (2007) 7075.
[26] J.D. Lawrence, H. Li, T.B. Rauchfuss, M. Bénard, M.-M. Rohmer, Angew. Chem., Int. Ed. 40 (2001) 1768.
[27] H. Li, T.B. Rauchfuss, J. Am. Chem. Soc. 124 (2002) 726.
[28] L.-C. Song, M.-Y. Tang, F.-H. Su, Q.-M. Hu, Angew. Chem., Int. Ed. 45 (2006) 1130.
[29] L.-C. Song, B.-S. Yin, Y.-L. Li, L.-Q. Zhao, J.-H. Ge, Z.-Y. Yang, Q.-M. Hu, Organometallics 26 (2007) 4921.
[30] L.-C. Song, J.-H. Ge, X.-G. Zhang, Y. Liu, Q.-M. Hu, Eur. J. Inorg. Chem (2006) 3204.
[31] T. Liu, M. Wang, Z. Shi, H. Cui, W. Dong, J. Chen, B. Åkermark, L. Sun, Chem. Eur. J. 10 (2004) 4474.
[32] D. Morvan, J.-F. Capon, F. Gloaguen, A.L. Goff, M. Marchivie, F. Michaud, P. Schollhammer, J. Talarmin, J.-J. Yaouanc, Organometallics 26 (2007) 2042.
[33] J.-F. Capon, S.E. Hassnaoui, F. Gloaguen, P. Schollhammer, J. Talarmin, Organometallics 24 (2005) 2020.
[34] J.W. Tye, J. Lee, H.-W. Wang, R. Mejia-Rodriguez, J.H. Reibenspies, M.B. Hall, M.Y. Darensbourg, Inorg. Chem. 44 (2005) 5550.
[35] S. Jiang, J. Liu, Y. Shi, Z. Wang, B. Åkermark, L. Sun, Polyhedron 26 (2007) 1499.
[36] T. Liu, M.Y. Darendbourg, J. Am. Chem. Soc. 129 (2007) 7008.
[37] A.J. Arduengo III, Acc. Chem. Res. 32 (1999) 913.
[38] W.A. Herrmann, J. Schütz, G.D. Frey, E. Herdtweck, Organometallics 25 (2006) 2437.
[39] L. Mercs, G. Labat, A. Neels, A. Ehlers, M. Albrecht, Organometallics 25 (2006) 5648.
[40] M. Viciano, E. Mas-Marzá, M. Sanau, E. Peris, Organometallics 25 (2006) 3063.
[41] L.-C. Song, Z.-Y. Yang, H.-Z. Bian, Y. Liu, H.-T. Wang, X.-F. Liu, Q.-M. Hu, Organometallics 24 (2005) 6126.
[42] L.-C. Song, Z.-Y. Yang, Y.-J. Hua, H.-T. Wang, Y. Liu, Q.-M. Hu, Organometallics 26 (2007) 2106.
[43] L.-C. Song, J.-H. Ge, X.-F. Liu, L.-Q. Zhao, Q.-M. Hu, J. Organomet. Chem. 691 (2006) 5701.
[44] L.-C. Song, M.-Y. Tang, S.-Z. Mei, J.-H. Huang, Q.-M. Hu, Organometallics 26 (2007) 1575.
[45] L.-C. Song, C.-G. Li, J. Gao, B.-S. Yin, X. Luo, X.-G. Zhang, H.-L. Bao, Q.-M. Hu, Inorg. Chem. 47 (2008) 4545.
[46] L.-C. Song, Acc. Chem. Res. 38 (2005) 21.
[47] A.J. Arduengo III, H.V. Rasika Dias, R.L. Harlow, M. Kline, J. Am. Chem. Soc. 114 (1992) 5530.
[48] P. Buchgraber, L. Toupet, V. Guerchais, Organometallics 22 (2003) 5144.
[49] L.-C. Song, J.-H. Ge, J. Yan, H.-T. Wang, X. Luo, Q.-M. Hu, Eur. J. Inorg. Chem. (2008) 164.
[50] J.P. Collman, L.S. Hegedus, Principles and Applications of Organotransition Metal Chemistry, University Science Books, California, 1980.
[51] M.G. Gardiner, W.A. Herrmann, C.-P. Reisinger, J. Schwarz, M. Spiegler, J. Organomet. Chem. 572 (1999) 239.
[52] J.L. Anderson, R. Ding, A. Ellern, D.W. Armstrong, J. Am. Chem. Soc. 127 (2005) 593.
[53] F. Gloaguen, J.D. Lawrence, T.B. Rauchfuss, J. Am. Chem. Soc. 123 (2001) 9476.
[54] D. Chong, I.P. Georgakaki, R. Mejia-Rodriguez, J. Sanabria-Chinchilla, M.P. Soriaga, M.Y. Darensbourg, Dalton Trans. (2003) 4158.
[55] R. Mejia-Rodriguez, D. Chong, J.H. Reibenspies, M.P. Soriaga, M.Y. Darensbourg, J. Am. Chem. Soc. 126 (2004) 12004.
[56] J.-F. Capon, F. Gloaguen, P. Schollhammer, J. Talarmin, Coord. Chem. Rev. 249 (2005) 1664.
[57] I. Bhugun, D. Lexa, J.-M. Saveant, J. Am. Chem. Soc. 118 (1996) 3982.
[58] J.P. Collman, Y. Ha, P.S. Wagenknecht, M.A. Lopez, R. Guilard, J. Am. Chem. Soc. 115 (1993) 9080.
[59] A.J. Arduengo III, R. Krafczyk, R. Schmutzler, H.A. Craig, J.R. Goerlich, W.J. Marshall, M. Unverzagt, Tetrahedron 55 (1999) 14523.
[60] J.D. Lawrence, H. Li, T.B. Rauchfuss, Chem. Commun. (2001) 1482.
[61] D. Seyferth, R.S. Henderson, L.-C. Song, J. Organomet. Chem. 192 (1980) C1.
[62] CrystalClear 1.3.6. Rigaku and Rigaku/MSC, 9009 New Trail Dr. The Woodlands, TX 77381, USA, 2005.
[63] G.M. Sheldrick, SADABS, A Program for Empirical Absorption Correction of Area Detector Data, University of Göttingen, Germany, 1996.
[64] G.M. Sheldrick, SHELXS-97, A Program for Crystal Structure Solution, University of Göttingen, Germany, 1997.
[65] G.M. Sheldrick, SHELXL-97, A Program for Crystal Structure Refinement, University of Göttingen, Germany, 1997.